Proceedings of the 21st ICSMGE, Vienna, Austria, 14 – 19 June 2026. Pistrol, Adam & Schweiger (eds.)
Published by: ÖGG, Austrian Society for Geomechanics, Salzburg, Austria, ISBN 978-3-9503898-4-5
https://doi.org/10.53243/ICSMGE2026-1409

The laterally stastic loading test of the rock-socketed closed diaphragm walls.

Zhenzhao Sun, Weiming Gong
School of Civil Engineering, Southeast University, Nanjing, Jiangsu, China, wmgong@seu.edu.cn

ABSTRACT: the rock-socketed closed diaphragm walls demonstrate superior horizontal stiffness and exceptional displacement control, leading to their extensive application in densely built urban areas. A comprehensive in-situ lateral static loading test was conducted on such walls at a construction site in Guangdong Province, China, with pre-installed displacement gauges monitoring cap-top displacements throughout the loading process. The maximum applied load reached 80500 kN, currently recognized as the world's largest-scale laterally static loading test. Critical findings reveal that the load-displacement curves exhibited a gradual nonlinear pattern, with peak displacements of 108.02 mm and 103.72 mm for the two test walls. The displacement control threshold (20 mm) was attained at applied loads of 35000 kN and 38500 kN, highlighting their early-stage stiffness advantage. Notably, the walls underwent vertical rotation during loading, with the rotation point located at a relatively shallow depth within the rock layer. The lateral geotechnical resistance along the wall first increased and then decreased with depth, with the maximum earth pressure occurring at about 0.28 times the wall depth.

KEYWORDS: Diaphragm walls, large foundation, lateral static loading test.

INTRODUCTION

Closed diaphragm walls serve as a foundation type frequently employed in large-scale construction projects in recent years (Cheng et al.,2012; Li et al., 2019; Zhang et al., 2021; Li et al., 2024). This method involves connecting individual wall panels underground via joints to form a continuous enclosing wall structure. Featuring high horizontal stiffness and excellent displacement control, enclosed diaphragm walls minimize the impact of new constructions on existing buildings in densely built areas (Jia et al., 2019; Wu et al., 2020; Wu et al., 2024). Specifically designed for the bedrock distribution characteristics of coastal Guangdong regions, the rock-socketed enclosed diaphragm wall utilizes structurally sound bedrock as its anchoring layer. This design significantly outperforms conventional enclosed diaphragm walls in both deformation control and load-bearing capacity.

This paper focuses on a proposed rock-socketed closed diaphragm wall scheme for a Guangdong project. Using large-scale horizontal loading equipment, full-scale rectangular rock-socketed closed diaphragm walls constructed on-site underwent lateral static load tests. Embedded instruments monitored changes in wall-top displacement during loading. The study analyzed the deformation characteristics of the rock-socketed enclosed diaphragm wall foundation under progressive horizontal loads. The results served both to inform safety-critical design decisions for this specific project and to provide guidance for future similar projects.

1 TEST OVERVIEW

1.1 *Project overview*

The test site was located in Guangdong Province, China. The loading was applied using a mutual pushing method between two diaphragm walls. Both test walls featured a rectangular box-type configuration, as shown in Figure 1, with plan dimensions of 8.2m × 6.6m. A 1.8m-thick cap slab was installed at the top (with 0.4m of wall embedded into the cap), and the bottom of each test wall section was socketed approximately 5m into bedrock.

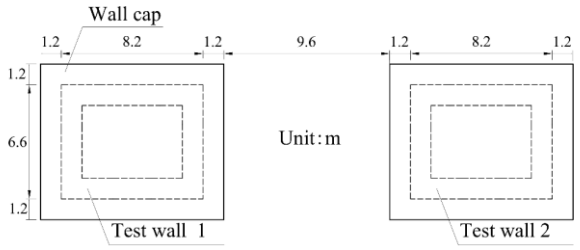

Figure 1. Schematic Plan View of Diaphragm Wall.

The site stratigraphy consisted of silty clay, gravelly cohesive soil, completely weathered granite, highly weathered granite, moderately weathered granite, and slightly weathered granite from top to bottom. Mechanical parameters for each soil and rock layer were determined based on the detailed investigation report, as listed in Table 1 and Table 2 respectively.

Table 1. Soil Parameters.

Soil Stratum	Unit Weight (kN/m3)	Cohesion (kPa)	Internal Friction Angle (°)
Silty Clay	17.8	33	24.7
Gravelly Clay	17.7	22.67	27.13
Completely Weathered Granite	19	22.87	28.05
Highly Weathered Granite	19	23.82	28.17

Table 2. Rock Parameters.

Rock Stratum	Uniaxial Compressive Strength (MPa)
Moderately Weathered Granite	15
Slightly Weathered Granite	40

1.2 *Test walls overview*

Each test wall was constructed using four L-shaped panels and two linear panels, with panel division details and dimensions illustrated in Figure 2. The wall depth design for each panel followed the principle of maintaining a five-meter rock socket depth. Consequently, wall depths were determined based on bedrock elevations obtained from borehole data, as

specified in Table 3. All wall sections utilized underwater C40-grade concrete.

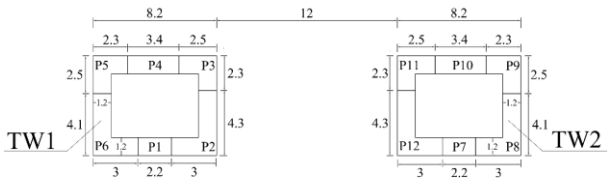

Figure 2. Panel layout diagram of diaphragm wall.

Table 3. Panel depth.

Panel	Depth (m)	Panel	Depth (m)
P1	24.92	P7	29.96
P2	27.51	P8	30.34
P3	28.31	P9	31.83
P4	29.44	P10	30.45
P5	29.87	P11	30.05
P6	28.92	P12	30.7

The test wall construction primarily involved four sequential stages: panel excavation, reinforcement cage fabrication, cage installation, and concrete pouring. A grab-clamshell and milling excavation combined technique was implemented: upper soil layers were excavated using grab-clamshell equipment, while bedrock layers were milled with hydraulic milling machines. Where bedrock proved exceptionally hard, rotary drilling rigs were employed for supplementary pilot hole drilling.

2 TEST PROCEDURE

2.1 *Loading method*

The loading system comprised eight horizontal hydraulic jacks (UH-11000/YG505-11000×1) with total assembly dimensions of 6.6m length × 1m height × 0.65m thickness; the spatial configuration of loading equipment, cap structure (1.8m thick extending 1.2m beyond wall peripheries on all sides with 0.4m wall-top embedment), and force transfer devices are detailed in Figure 3, where reinforced concrete transfer assemblies incorporated steel pipes beneath to reduce soil friction.

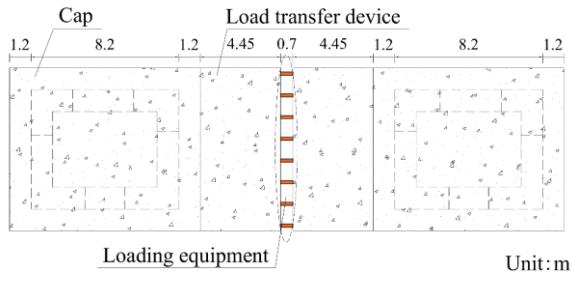

Figure 3. Field setup layout for loading test.

2.2 *Instrumentation scheme*

To monitor the displacement at the wall cap top during the test and obtain the load-displacement curve during loading, electronic displacement transducers were installed at the top of the wall cap.

For the transducer placement, four measurement points were selected on the wall cap tops of the two test walls, as illustrated in Figure 4. On the front wall (the side facing the loading direction), displacement transducers were placed both at the wall cap top and 50 cm below it. On the rear wall, displacement transducers were installed only at the wall top. A total station was used to monitor key locations on the wall cap top to verify the reliability of the displacement transducer data.

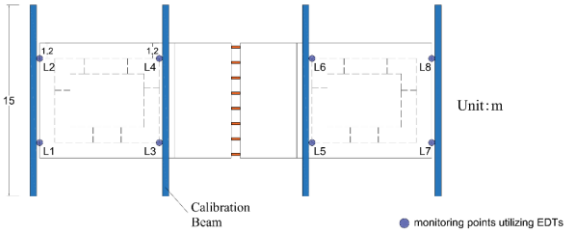

Figure 4. Panel layout diagram of diaphragm wall.

To investigate the vertical distribution of earth pressure, ten earth pressure cells (EPCs) were installed at each monitoring point on Faces A and H, while seven EPCs were installed at the remaining points. The vertical layout of these sensors is illustrated in Figure 5.

A total of 158 EPCs were deployed across the two test walls. To specifically evaluate the influence of the socketed rock layer on wall behavior, at least three EPCs at each monitoring point were positioned below the rock surface to measure the rock resistance.

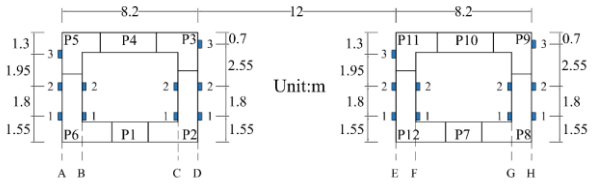

Figure 5. Plan layout of EPCs.

The EPCs embedded in the soil layers had dimensions of 118 mm × 123 mm × 29.5 mm with a measurement range of 1 MPa, whereas those installed in the rock layers measured 198 mm × 203 mm × 34 mm with a range of 2 MPa.

2.3 *Loading procedure*

The laterally stastic loading test of the diaphragm wall commenced at 12:20 on March 14, 2024 (73 days after wall casting completion). The loading protocol consisted of 23 incremental stages, each applying 3,500 kN, with the loading sequence detailed in Table 4.

Table 4. Loading Stages.

Stage	Load (kN)	Stage	Load (kN)
1	3500	13	45500
2	7000	14	49000
3	10500	15	52500
4	14000	16	56000
5	17500	17	59500
6	21000	18	63000
7	24500	19	66500
8	28000	20	70000
9	31500	21	73500
10	35000	22	77000

11	38500	23	80500
12	42000		

Testing concluded at 09:00 on March 24, 2024, reaching a peak load of 80500 kN. To our knowledge, this represents the world's largest horizontally loaded static test to date. Field documentation of the test procedure is provided in Figure 6.

Figure 6. Test Site.

3 ANALYSIS OF TEST RESULTS

3.1 *Load-displacement curve*

In the subsequent analysis, the side designated as L1-L3-L5-L7 is referred to as Side A, with the opposing side defined as Side B.

Load-displacement curves at the wall cap tops of Test Walls TW1 and TW2 are presented in Figure 7 and Figure 8, respectively. All monitored curves exhibit nonlinear behavior without abrupt drops during loading, demonstrating a gradually progressive pattern. During the first five loading stages (≤17500 kN), the curves approximate linear relationships, indicating near-linear elastic states in both wall deformation and soil-structure interaction. Beyond the sixth stage (21000 kN), increasing nonlinearity emerges as curve slopes progressively decrease.

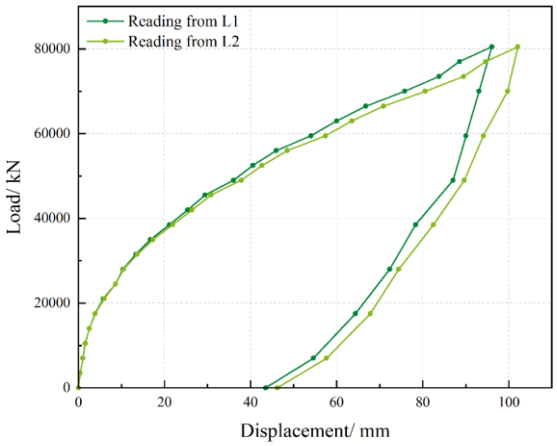

(a) front wall

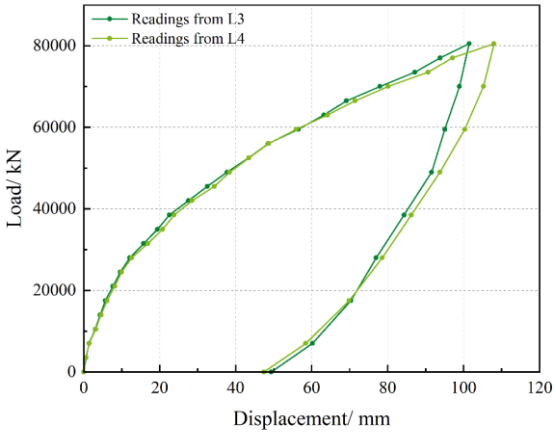

(b) rear wall

Figure 7. Load-Displacement Curve for Test Wall TW1.

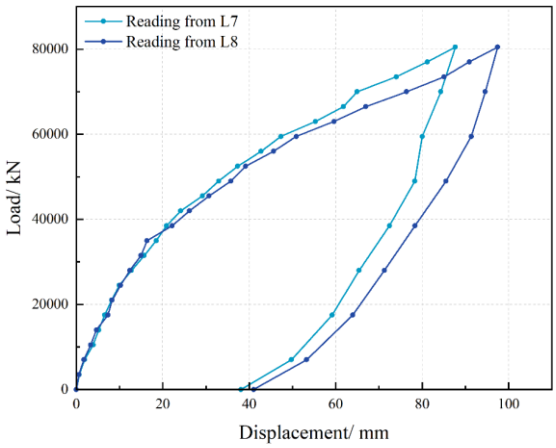

(a) front wall

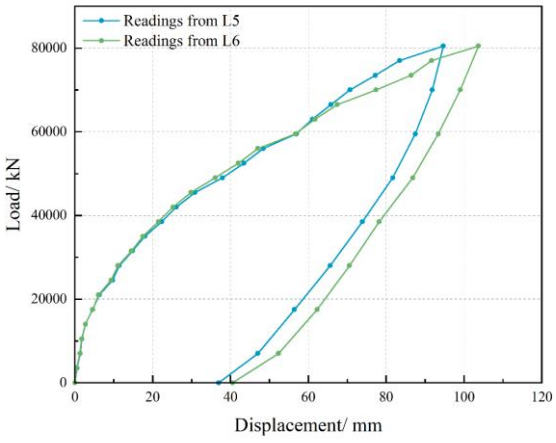

(b) rear wall

Figure 8. Load-Displacement Curve for Test Wall TW2.

At the peak load of 80500 kN, maximum displacements occurred at Side A of the rear wall for both TW1 (108.02 mm) and TW2 (103.72 mm).

According to the design requirements of the underlying project, analyses were performed for two displacement control thresholds (2 cm and 5 cm). At 35000 kN loading, the displacement at monitoring point L4 of Test Wall TW1 reached 20.8 mm, while no monitoring points on TW2 exceeded the 2 cm threshold. Upon increasing the load to 38,500 kN,

displacements at points L5 and L6 of TW2 surpassed 2 cm, recording 22.35 mm and 21.49 mm, respectively. Both walls simultaneously reached the 5 cm displacement threshold at 59500 kN, with maximum displacements of 56.49 mm (TW1) and 56.92 mm (TW2), both occurring at Side A of the rear wall.

3.2 *Earth and rock pressure*

The locations of the pressure cells embedded in the test wall are shown in Figure 5. In line with the research focus of this paper, the analysis mainly concentrates on the pressure cells at points A-2, B-2, C-2, and D-2 on test wall TW1. For ease of description, the pressure cells at different depths at these points are numbered as shown in Figure 9.

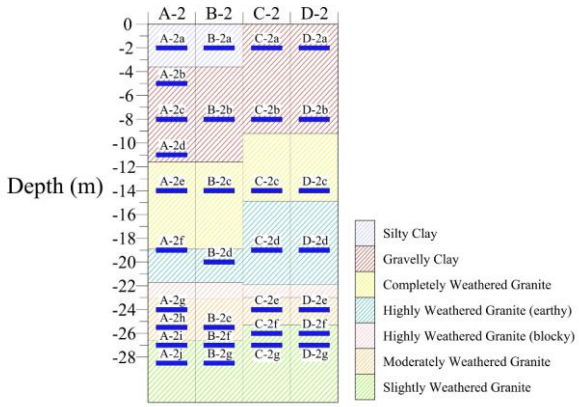

Figure 9. Installation profile of pressure cells.

Figure 10 presents the depthwise distributions of the lateral geotechnical resistance (measured by the pressure cells) at point A-2 under different load levels. At low loads, resistance is mobilized only in the shallow soil. As the load increases, the load is gradually transferred to greater depths and the deeper soil/rock begins to provide resistance. When the load reaches 80,500 kN, the earth pressure first increases and then decreases with depth. The maximum pressure occurs in the gravelly clay at a depth of about 8 m, with a peak value of 383 kPa. It then decreases with depth; the pressures at 14 m (completely weathered granite) and 19 m (highly weathered granite) are 334 kPa and 185 kPa, respectively.

As shown in the figure, the rockhead at point A-2 is at a depth of 23 m. The readings from A-2g (24 m), A-2h (25.5 m), A-2i (27 m), and A-2j (28.5 m) represent rock resistance. Among them, A-2g is located in moderately weathered granite, while the others are in slightly weathered granite. Although the wall displacement in the rock-socketed segment is very small, the stiffness of rock is much higher than that of soil; therefore, the rock resistance measured at A-2g is 181 kPa, which is close to the soil resistance at 19 m. The rock resistance measured by the deeper cells is zero, indicating that the wall's rotation point lies between 24 m and 25.5 m, i.e., at a relatively shallow level within the rock layer.

Pressure cells A-2a (2 m) and A-2b (5 m) are located in silty clay and gravelly clay, respectively. Their measured soil resistance tends to stabilize after the load reaches 66,500 kN, fluctuating around 240 kPa and 370 kPa, respectively, indicating that the soil at these depths has reached the ultimate lateral resistance. Pressure cell A-2c (8 m) is also located in the gravelly clay; however, even at 80,500 kN it has not reached the ultimate lateral resistance, and the measured resistance is 383 kPa. This suggests that, even within the same soil layer, the ultimate lateral resistance varies with embedment depth, mainly due to differences in confining pressure. The deeper pressure cells continue to increase, indicating that the deeper soil/rock has not yet reached ultimate lateral resistance.

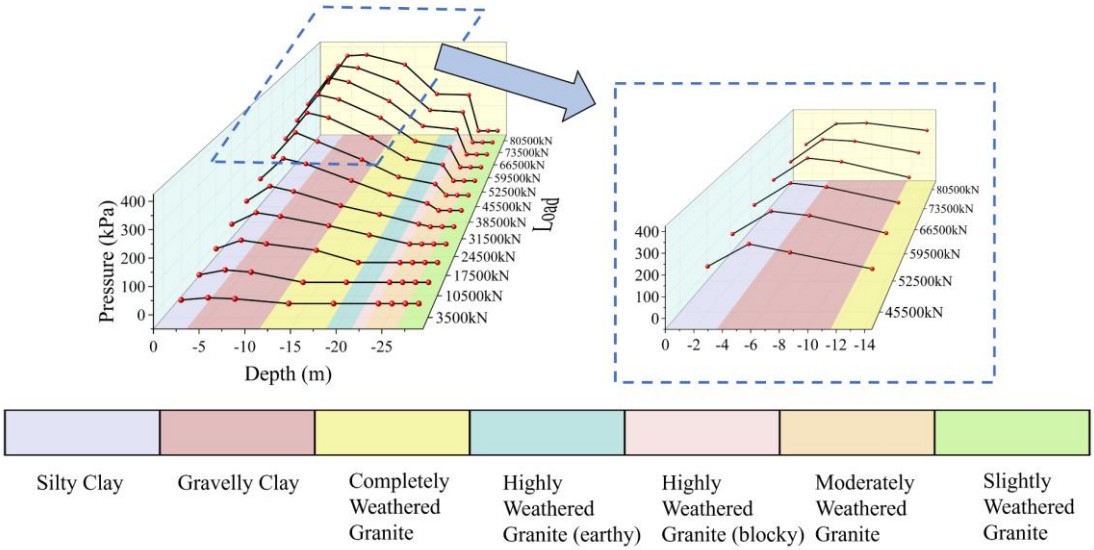

Figure 10. Earth and rock pressure distribution curves at position A-2.

Figure 11 presents the depthwise distributions of geotechnical resistance at points B-2, C-2, and D-2 under different load levels.

Figures (a) and (b) show the depthwise distributions of geotechnical resistance at points B-2 and D-2, respectively, under different load levels. It can be seen that the soil resistance at all depths at B-2 and D-2 is zero, whereas the rock resistance in the bottom rock layer is relatively large.

Pressure cell B-2e (24 m) is located in moderately weathered granite, while B-2f (25.5 m) and B-2g (27 m) are located in slightly weathered granite. At 80,500 kN, the rock resistances measured by B-2e, B-2f, and B-2g are 36 kPa, 258 kPa, and 495 kPa, respectively. Pressure cells D-2e (24.5 m) and D-2f (25.5 m) are located in moderately weathered granite and slightly weathered granite, respectively; at 80,500 kN, the measured rock resistances are 106 kPa and 410 kPa.

Comparing the rock resistance at the same depth for the two points, the rock resistances measured by B-2f and D-2f at 25.5 m are 258 kPa and 495 kPa, respectively; the rock resistance at B-2 is significantly smaller than that at D-2 at the

same depth. Therefore, it can be inferred that the rock mass inside the caisson is affected by size effects and related factors, and the rock resistance of slightly weathered granite inside the caisson is approximately 0.63 times that outside the caisson.

Figure (c) shows the depthwise distribution of geotechnical resistance at point C-2 under different load levels. The soil resistance in the soil layers is zero, indicating that the soil inside the caisson deforms together with the wall and does not interact with the wall. The resistance of the moderately weathered granite measured by C-2e (24 m) is 133 kPa. At the same depth outside the caisson (A-2g), the rock resistance is 181 kPa, indicating that the rock resistance of moderately weathered granite inside the caisson is approximately 0.73 times that outside the caisson.

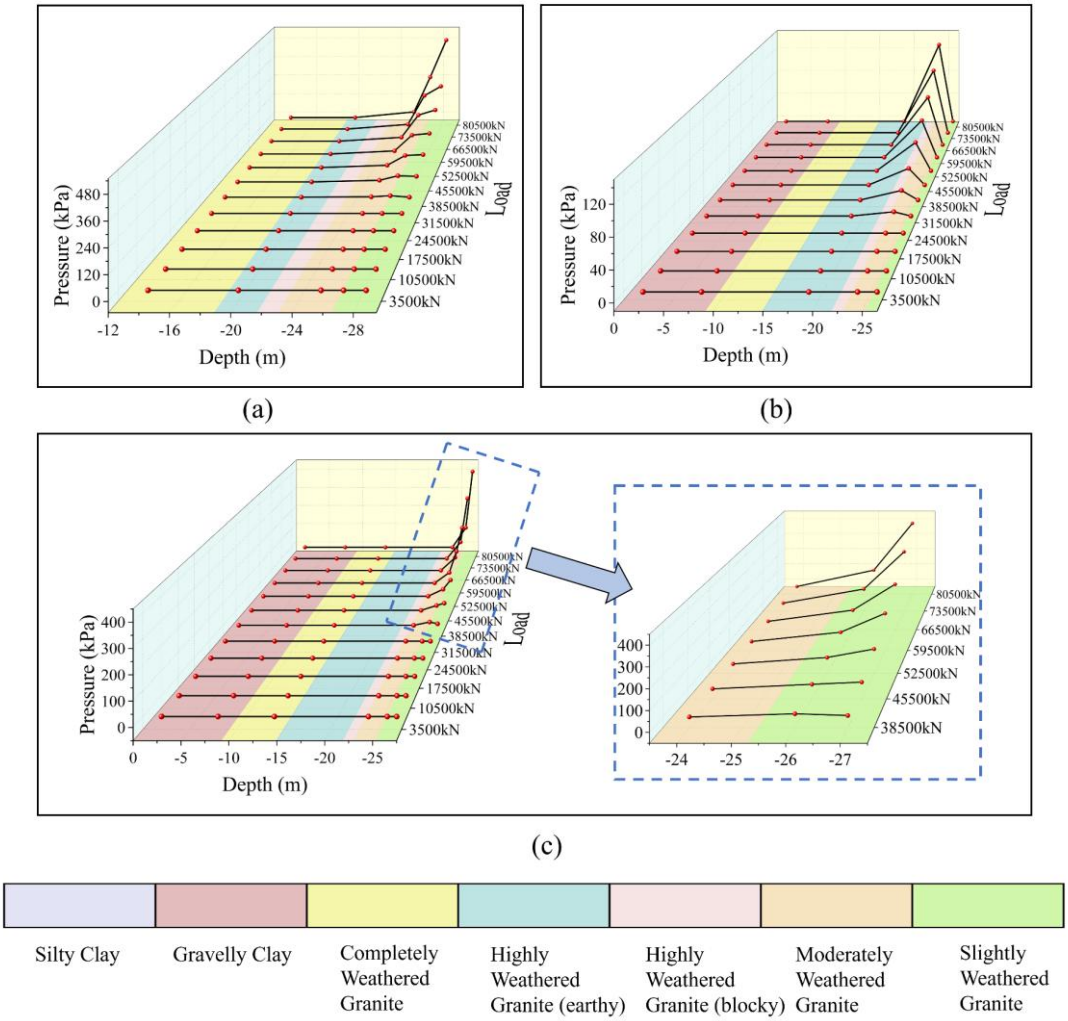

Figure 11. Earth and rock pressure distribution curves.

Based on the above analyses of geotechnical resistance distributions at these three locations, under horizontal loading the soil inside the caisson deforms compatibly with the wall, and no lateral soil resistance is mobilized along the wall; thus, the soil inside the caisson does not contribute to the load-bearing performance of the diaphragm wall. In contrast, the rock mass inside the caisson does provide resistance; however, due to size effects and other factors, the rock resistance is reduced compared with that outside the caisson. Specifically, the resistance of moderately weathered granite inside the caisson is approximately 0.73 times that outside the caisson, and the resistance of slightly weathered granite inside the caisson is approximately 0.63 times that outside the caisson.

4 CONCLUSIONS

At this study conducted an in-situ horizontally loaded test on rock-socketed closed diaphragm walls, monitoring wall cap top displacements and geotechnical resistance via pre-installed transducers during loading. Key conclusions are summarized as follows:

(1) The load-displacement curves exhibit gradually progressive nonlinear behavior without abrupt drops during loading. At the ultimate load of 80500 kN, maximum displacements reached 108.02 mm (TW1) and 103.72 mm (TW2).

(2) The 20-mm displacement control threshold was triggered at 35000 kN (TW1) and 38500 kN (TW2), while the 50-mm threshold was simultaneously achieved by both walls at 59500 kN.

(3) Vertical rotations occurred during loading, with rotation centers located at shallow positions within bedrock formations.

(4) At the initial stage of loading, resistance was mobilized only in the shallow soil. With increasing load, the deeper soil–rock layers gradually began to mobilize resistance. At all monitoring points, the geotechnical resistance increased first and then decreased with depth. The maximum soil resistance occurred at an embedment depth of 6.5 m below the wall top, i.e., at about 0.23 times the wall depth. During loading, only the soil–rock layers within 3.5 m below the wall top reached the ultimate lateral resistance.

(5) The soil inside the caisson deformed compatibly with the wall, and no soil resistance was recorded on the inner side of the wall. In contrast, the rock mass inside the caisson did provide resistance; however, the rock resistance at the same depth differed markedly between the inside and outside of the caisson. The resistance of moderately weathered granite inside the caisson was approximately 0.73 times that outside the caisson, and the resistance of slightly weathered granite inside the caisson was approximately 0.63 times that outside the caisson.

5 ACKNOWLEDGEMENTS

This work was supported by the National Natural Science Foundation of China (No. 52178317). The authors wish to express their sincere thanks to the people concerned.

6 REFERENCES

Cheng, Q., Wu, J., Song, Z., & Wen, H. (2012). The behavior of a rectangular closed diaphragm wall when used as a bridge foundation. *Frontiers of Structural and Civil Engineering*, *6*(4), 398-420.

Li, Y., Cheng, Q. G., Zhang, J. L., Lyu, B., Wang, Y. F., & Wu, J. J. (2019). Seismic behavior of rectangular closed diaphragm walls in gently sloping liquefiable deposit: dynamic centrifuge testing. Journal of Geotechnical and Geoenvironmental Engineering, 145(12), 04019105.

Jia, J., Zhai, J. Q., Li, M. G., Zhang, L. L., & Xie, X. L. (2019). Performance of large-diameter circular diaphragm walls in a deep excavation: Case study of Shanghai Tower. *Journal of Aerospace Engineering*, *32*(5), 04019078.

Wu, J., El Naggar, M. H., Cheng, Q., Wen, H., Li, Y., & Zhang, J. (2020). Iterative load transfer procedure for settlement evaluation of lattice-shaped diaphragm walls in multilayered soil. *Computers and Geotechnics*, *120*, 103409.

Zhang, J. L., Cheng, Q. G., Li, Y., Zhang, E. M., Wang, Y. F., Wu, J. J., & Xie, S. Y. (2021). Mechanism of liquefaction mitigation by rectangular closed diaphragm walls in sloping liquefiable deposits. *Soil Dynamics and Earthquake Engineering*, *142*, 106582.

Li, W., Tao, Q., Li, C., Wang, X., Gong, W., & Dai, G. (2024). In-situ experimental study of closed-diaphragm wall foundations for cross-sea suspension bridges. *Journal of Marine Science and Engineering*, *12*(12), 2304.

Wu, J., Hu, H., Pu, L., Mase, L. Z., & Jongpradist, P. (2024). Experimental investigation on the lateral bearing behavior of lattice-shaped diaphragm wall with double-layer configuration. *Frontiers of Structural and Civil Engineering*, *18*(12), 1815-1828.